Astron. Astrophys. 269, 39–53 (1993)

ASTRONOMY AND ASTROPHYSICS

Spectroscopic monitoring of active galactic nuclei*

II. The Seyfert-1 galaxy NGC 3516

I. Wanders[1], E. van Groningen[1], D. Alloin[2], I. Aretxaga[3], D. Axon[4], A.G. de Bruyn[5], J. Clavel[6], M. Dietrich[7], M.R. Goad[8], P. Gondhalekar[9], K. Horne[10], N. Jackson[11], W. Kollatschny[7], E. Laurikainen[12], A. Lawrence[13], J. Masegosa[14], P.T O'Brien[8], A. del Olmo[14], M.V. Penston[15], J. Perea[14], E. Pérez[16], I. Pérez-Fournon[16], J.J. Perry[17], A. Robinson[17], J.M. Rodriguez Espinosa[16], G.M. Stirpe[18], C. Tadhunter[19], R. Terlevich[15], S. Unger[15], S.J. Wagner[20] and R. Williams[17]**

[1] Astronomiska observatoriet, Box 515, S-75120 Uppsala, Sweden
[2] Observatoire de Paris, Place Jules Janssen, F-92195 Meudon Principal Cedex, France
[3] Dpto. Física Teórica, C-XI, Univ. Autonoma de Madrid, E-28049 Madrid, Spain
[4] NRAL, Jodrell Bank, Macclesfield, Cheshire SK11 9DL, United Kingdom
[5] Radiosterrewacht, Postbus 2, NL-7990 AA Dwingeloo, The Netherlands
[6] ESA Astrophysics Division, ESTEC, Postbus 299, NL-2200 AG Noordwijk, The Netherlands
[7] Universitäts-Sternwarte, Geismarlandstraße 11, W-3400 Göttingen, Germany
[8] Department of Physics and Astronomy, UCL, Gower Street, London WC1E 6BT, United Kingdom
[9] Rutherford Appleton Laboratory, Chilton, Didcot, Berks OX1 0QX, United Kingdom
[10] Space Science Telescope Institute, 3700 San Martin Drive, Baltimore, MD 21218, USA
[11] Sterrewacht Leiden, Postbus 9513, NL-2300 RA Leiden, The Netherlands
[12] Turku University Observatory, Tuorla, SF-21500 Piikkiö, Finland
[13] Queen Mary College, University of London, Mile End Road, London E1, United Kingdom
[14] Instituto de Astrofísica de Andalucía, Apartado 2144, E-18080 Granada, Spain
[15] Royal Greenwich Observatory, Madingley Road, Cambridge CB3 0EZ, United Kingdom
[16] Instituto de Astrofísica de Canarias, E-38200 La Laguna, Tenerife, Spain
[17] Institute of Astronomy, Madingley Rd., Cambridge CB3 0HA, United Kingdom
[18] Osservatorio Astronomico di Bologna, Via Zamboni 33, I-40126 Bologna, Italy
[19] Department of Physics, Hounsfield Rd., Sheffield S3 73H, United Kingdom
[20] Landessternwarte, Königstuhl, W-6900 Heidelberg, Germany

Received August 26, accepted November 4, 1992

Abstract. We present results of a five month spectroscopic monitoring campaign of the Seyfert-1 galaxy NGC 3516. Using a new calibration method and applying a correction for seeing differences during the various observations we can scale the spectra to each other with a much higher accuracy than hitherto achieved. NGC 3516 shows large amplitude variations on a time scale of several weeks. Asymmetric profile variations occur on the same time scale as the continuum variations. We show the presence of a varying dip on the blue wing of the Hβ profile, which is not present on the Hα profile, and which corresponds to the absorption features previously seen in the UV emission lines of NGC 3516. From cross-correlation analysis we find a time lag of 14 ± 2 days for the Hα and 7 ± 3 days for the Hβ emission-line response to continuum variations.

Key words: data analysis – galaxies: NGC 3516 – galaxies: Seyfert – lines: profile – spectroscopy

Send offprint requests to: I. Wanders

* This article is based on work carried out by the LAG (Lovers of Active Galaxies) collaboration. LAG is a consortium of mainly European astronomers which was established to study active galaxies using the International Time allocation at the Canary Islands' observatories operated under the auspices of the Comité Científico Internacional.

** Deceased 22 December 1990

1. Introduction

NGC 3516 was the first Seyfert-1 galaxy shown to vary in its broad-line flux (Andrillat & Souffrin 1968). Since then many Seyfert-1 galaxies have been reported to be variable and variability seems to be a common property of many active galactic nuclei (AGN).

In the standard model the broad-line region (BLR) is made up of a large number of small clouds at a certain range of distances from the central continuum source. The clouds are photoionized by the bright continuum source and respond to changes in the ionizing flux. The clouds' response (the broad-line emission) equals the variations in ionizing flux convolved with some unknown transfer function, which depends on the distribution and the kinematics of the clouds as well as the physical conditions in the clouds. By monitoring both ionizing flux and line emission variations we can in principle recover the transfer function of the BLR by reverberation mapping (Blandford & McKee 1982; Pérez et al. 1991; Welsh & Horne 1991) and put constraints on the physical models of the BLR.

Several Seyfert-1 galaxies have been subject to such monitoring projects (Clavel et al. 1990; Maoz et al. 1991; Peterson et al. 1991; Peterson et al. 1993) but generally the resolution of these data is too low to allow the recovery of the full two-dimensional transfer function. Stirpe et al. (1988) showed that high resolution spectra are necessary to calibrate a series of spectra accurately by using the constant narrow emission lines as internal calibrators. This prompted a monitoring campaign with the aim of obtaining high S/N spectra with a resolution of $\sim$ 3Å in order to put stringent constraints on the transfer function. NGC 3516 was selected on the basis of its variability record and its brightness.

NGC 3516 is a type SB0 galaxy with redshift $z = 0.009$, visual magnitude $m_v = 12.5$ (but variable!) and its coordinates on the sky are $\alpha(2000.0) = 11^h06^m47^s.3$, $\delta(2000.0) = +72°34'12''$.

In Sect. 2 we briefly describe the observations that have been carried out. In Sect. 3 we give a detailed account of the data reduction, which is not trivial for this particular object. In Sect. 4 we present some results and discuss these briefly. Section 5 summarizes the main points.

2. The observations

During the first five months of 1990, NGC 3516 was monitored spectroscopically and photometrically as part of the LAG (Lovers of Active Galaxies) collaboration (Jackson et al. 1992), which was awarded the 5% international time on all telescopes on La Palma between March 1989 and September 1990. For the monitoring of the broad Hα and Hβ emission lines of NGC 3516, the 2.5m Isaac Newton Telescope (INT) and the 4.2m William Herschel Telescope (WHT) were used. In total, we obtained 22 Hα epochs and 21 Hβ epochs. On the WHT we used a 500mm camera and an EEV CCD. On the INT we used both the 235mm and the 500mm camera with a GEC CCD. We observed NGC 3516 using a slit of width 1.″5 at a position angle of 25° centred on the object. A summary of the observing schedule is given in Table 1a. Column 1 gives the Gregorian date of the beginning of the observing night in 1990, column 2 the telescope and column 3 the camera used, columns 4 and 6 the Julian date −2440000 of the centre of the observation for Hα and Hβ respectively, and columns 5 and 7 the exposure times in seconds. Especially during the first two months we got a very good time coverage and obtained high S/N spectra every 4 or 5 days. Unfortunately, a bad-weather period in March through May introduced large gaps in our time series.

For the photometric monitoring we used the 1.0m Jacobus Kapteyn Telescope (JKT) with either a GEC CCD, which had a

Table 1a. The spectral observations on the INT and WHT

			Hα		Hβ	
Date (1990)	Tel.	Cam. (mm)	JD -2440000	Exp (s)	JD -2440000	Exp (s)
2 Jan	INT	235	7894.581	900	7894.588	2000
5 Jan	INT	235	7897.608	900	–	–
10 Jan	INT	235	7902.577	900	7902.599	1800
19 Jan	INT	500	7911.603	900	7911.626	2000
19 Jan	WHT	500	7911.682	500	7911.661	1200
28 Jan	INT	500	7920.514	900	7920.637	2000
31 Jan	WHT	500	7923.613	400	7923.597	1200
5 Feb	INT	500	7928.622	900	7928.643	2000
8 Feb	INT	500	7931.560	900	7931.599	2000
11 Feb	INT	500	7934.472	900	7934.495	2000
16 Feb	WHT	500	7939.544	300	7939.562	700
21 Feb	INT	235	7944.585	900	7944.609	2000
6 Mar	INT	235	7957.482	900	7957.506	2000
24 Mar	WHT	500	7975.482	300	7975.614	700
31 Mar	WHT	500	7982.583	500	7982.643	300
2 Apr	WHT	500	7984.484	300	7984.489	500
13 Apr	INT	500	7995.437	900	7995.460	2000
15 Apr	INT	500	7997.416	900	7997.442	2000
2 May	WHT	500	8014.420	300	8014.405	700
13 May	WHT	500	8025.436	300	8025.413	700
20 May	INT	235	8032.401	900	–	–
24 May	WHT	500	–	–	8036.419	700
4 Jun	INT	500	8047.385	900	8047.410	2000

Table 1b. The photometric observations on the JKT

Date (1990)	JD -2440000	star1	star2	NGC 3516	seeing (″)	galaxy/ star1
2 Jan	7894.50	598.5	70.7	1266.	2.8	2.11
5 Jan	7897.50	373.0	–	758.	1.1	2.03
15 Jan	7907.50	535.0	61.2	1223.	2.2	2.29
18 Jan	7910.50	434.0	51.9	1002.	2.2	2.31
24 Jan	7916.50	450.0	53.3	969.	2.6	2.15
31 Jan	7923.50	447.0	51.7	997.	1.6	2.23
5 Feb	7928.50	249.0	32.9	579.	1.7	2.33
8 Feb	7931.50	514.0	63.0	1187.	1.4	2.31
11 Feb	7934.50	520.0	61.5	1105.	1.6	2.12
16 Feb	7939.45	447.0	54.7	923.	1.7	2.06
16 Feb	7939.55	450.0	54.4	913.	1.9	2.03
21 Feb	7944.50	524.0	63.5	1019.	2.5	1.94
13 Mar	7964.50	488.0	57.8	883.	1.6	1.81
29 Apr	8011.50	479.0	57.4	1078.	1.9	2.25
18 May	8030.50	105.0	12.8	260.	1.5	2.47
27 May	8039.50	431.0	–	1150.	1.1	2.67

field of $117'' \times 175''$, or a RCA CCD, which had a field of $132'' \times 212''$. These observations were done using a Johnson-B filter. On seven nights the JKT was used nearly simultaneously with either the INT or the WHT. In total we obtained 16 useful epochs on the JKT for NGC 3516. A summary of the JKT observations is given in Table 1b, where column 1 gives the Gregorian date of the beginning of the observing night in 1990 and column 2 gives the Julian date of the observation.

3. Data reduction

3.1. The standard reduction

The CCD frames from the photometry were bias and flat-field corrected. No absolute photometry was possible. However, beside NGC 3516 the field also contains two comparison stars which made differential photometry possible. We used a circular soft-ware aperture of $5''$ within which all flux as measured from the CCD frame was added to yield the total flux of the two comparison stars and the nucleus of NGC 3516. The seeing during the observations, as derived from the two comparison stars was always less than $2''.8$ FWHM and thus an aperture of $5''$ is sufficient. A larger aperture would only include more starlight from the bulge of NGC 3516 and dilute the variations from the nuclear source. The flux ratio of the two comparison stars is constant over the observations to within 3.3% r.m.s. The JKT-derived light curve of NGC 3516 was deduced from dividing the nuclear counts by the brightest-star counts. Background and flat-field analysis of the CCD frames yields an error on the light curve of 3%. These data are presented in Table 1b. Here, columns 3, 4 and 5 give the counts of the two comparison stars and the nucleus of NGC 3516, respectively, measured with a $5''$ aperture. Column 6 shows the FWHM of the seeing disc as deduced from the two standard stars and column 7 gives the nuclear flux of NGC 3516 relative to the brightest comparison star, which we adopt as the B-band light curve.

The standard reduction of the spectrometric data was done using the MIDAS package. The bias was subtracted from all frames and the frames were flat-field corrected. Every object frame had its accompanying CuNe or CuAr arc frame which was used for the wavelength calibration. All object and standard-star frames were cleaned manually from cosmic rays except in those cases where these fell on any important features like emission lines, extended narrow-line region (NLR) or nuclear continuum. We subtracted the night-sky spectrum from all frames; care was taken not to include any significant amount of galaxy light. We rebinned the frames to a common linear wavelength scale from 4500Å to 5500Å for the Hβ and 6200Å to 7200Å for the Hα spectra, with an increment of 1Å per pixel. The standard stars HD 84937 and BD +26°2606 were used for flux calibrating the spectra with the flux tables presented by Oke & Gunn (1983). Atmospheric B-band correction of the Hα spectra was done in the following way. We interpolated the standard star spectrum at the wavelengths of the atmospheric B-band.We then divided the standard-star spectrum by the interpolated one to get a correction spectrum which is everywhere unity except at the B-band. We divided the Hα spectra by this correction spectrum taking into account the difference in airmass during the observation of the two spectra. The nuclear Hα and Hβ spectra were then obtained by summing all flux within a distance of $1''$ of the centre. In this way our integrating aperture was $2'' \times 1''.5$.

3.2. The underlying galaxy

Due to the low contrast between the central continuum source and the underlying stellar spectrum a significant amount of starlight from the central regions of the bulge of the galaxy is included in the nuclear spectra. Since we want to measure the nonstellar continuum only, the amount of starlight must be estimated and subtracted.

The Hα spectra show no strong stellar absorption features but fortunately the Hβ spectra do show clear absorption lines such as the Mg b lines which can easily be identified. This gives us the possibility of subtracting a galaxy template spectrum such that all stellar absorption features disappear and we are left with a pure nonstellar-continuum spectrum. To construct a suitable galaxy template spectrum, we added 6 INT 2D-spectra (2 Jan, 28 Jan, 11 Feb, 21 Feb, 6 Mar, 4 Jun) of good quality and we added the off-nuclear columns – between $3''$ and $6''$ away from the nucleus – to obtain a spectrum of the bulge of NGC 3516. We made sure that the columns used were not contaminated with scattered broad line emission. The resulting template has a higher S/N but a slightly lower resolution than any of the individual object frames. At the wavelengths of the narrow emission lines we interpolated linearly under the extended narrow emission lines which still adorned our galaxy template spectrum. The extracted galaxy template spectrum is shown in Fig. 1.

The stellar absorption features, especially the Mg b lines, can clearly be identified. This galaxy spectrum appears bluer than that observed in the nucleus of a normal galaxy of the same type as NGC 3516 (Bica 1988). From the low level of contamination by diffuse light from the AGN, which is attested by the lack of broad line emission, we are led to believe that some recent star formation might have occurred in the bulge of NGC 3516. Assuming that the stellar population of the bulge is representative of the total stellar contribution to the nuclear spectra, we can subtract the galaxy template spectrum from all Hβ spectra after scaling the former appropriately in order to minimize the absorption-line residuals. For this procedure we used a computer algorithm based on a χ^2–test of which a short description is given in Sect. 3.3. The stellar contribution to the total extracted continuum is generally found to be around 50% but is as high as 74% in one case (15 April) and 72% in another (6 March). On these dates, the nonthermal continuum was in a very low state. The combination of varying seeing conditions from epoch to epoch and a varying nonthermal continuum makes it very difficult to subtract the stellar component from the total continuum other than by fitting a template to galactic absorption lines. An example of this fitting is given in Fig. 2 where a spectrum before and after galaxy subtraction is shown.

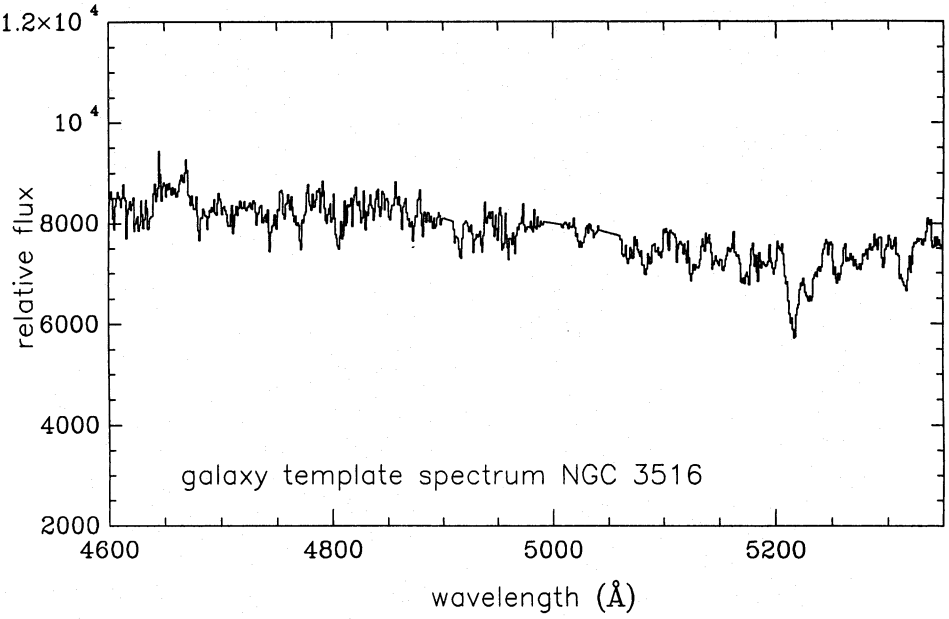

Fig. 1. The galaxy template spectrum of the bulge of NGC 3516

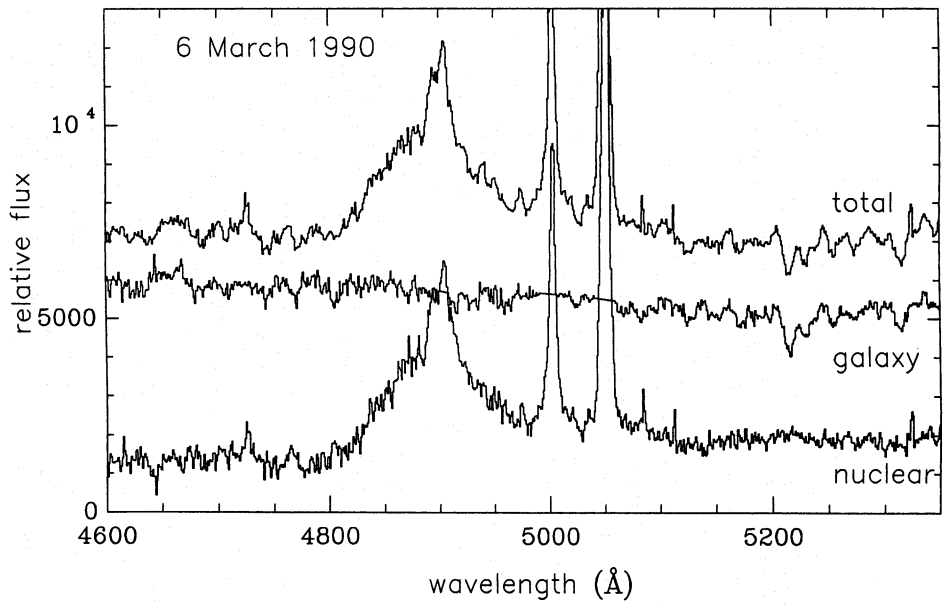

Fig. 2. Hβ spectrum of 6 March 1990 before and after the underlying galaxy was subtracted

3.3. Relative scaling of the spectra

We have now obtained two series of nuclear spectra: one Hβ series with the underlying galaxy spectrum eliminated and an Hα series still including the underlying galaxy spectrum. We now make the usual assumption that the narrow forbidden lines are constant over the time scale of interest (5 months) and use the [O III] and [S II] lines as internal flux calibrators to scale the spectra to each other. We will briefly describe the computer algorithm used, of which a full account and a detailed analysis can be found elsewhere (van Groningen & Wanders 1992). The scaling procedure has been automated to do this as objectively as possible. We did not fit the narrow-line fluxes as is commonly done because of the problem of estimating the local continuum level, which is the main cause of uncertainty in this scaling procedure (Baribaud & Alloin 1990). Instead we used difference spectra so that the method is insensitive to the continuum.

There are three free parameters in the scaling problem: flux scaling factor, wavelength shift (two spectra are never perfectly aligned) and resolution (different instruments used from one spectrum to the other plus seeing effects). The computer algorithm works as follows. One, high S/N spectrum with mediocre resolution is taken as a reference spectrum (in this case 4 June) and *all* other spectra are scaled to this one. The three free parameters form the sides of a datacube. For each voxel (volume element) its defining parameter values are used to create a difference spectrum of the spectrum we are scaling and the reference spectrum. We then fit the wavelength region in which the narrow lines lie with a second order polynomial and the χ^2 of this fit is calculated. Any narrow-line residuals will influence this χ^2

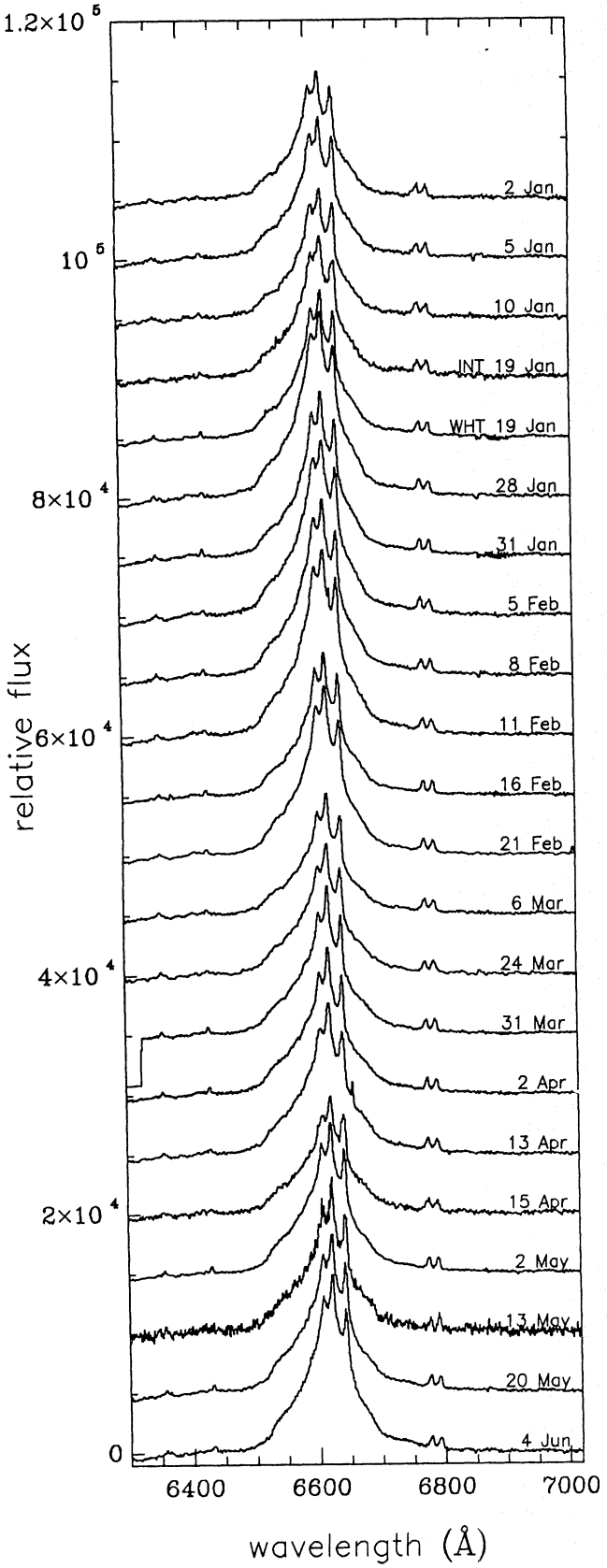

Fig. 3. The Hα spectra

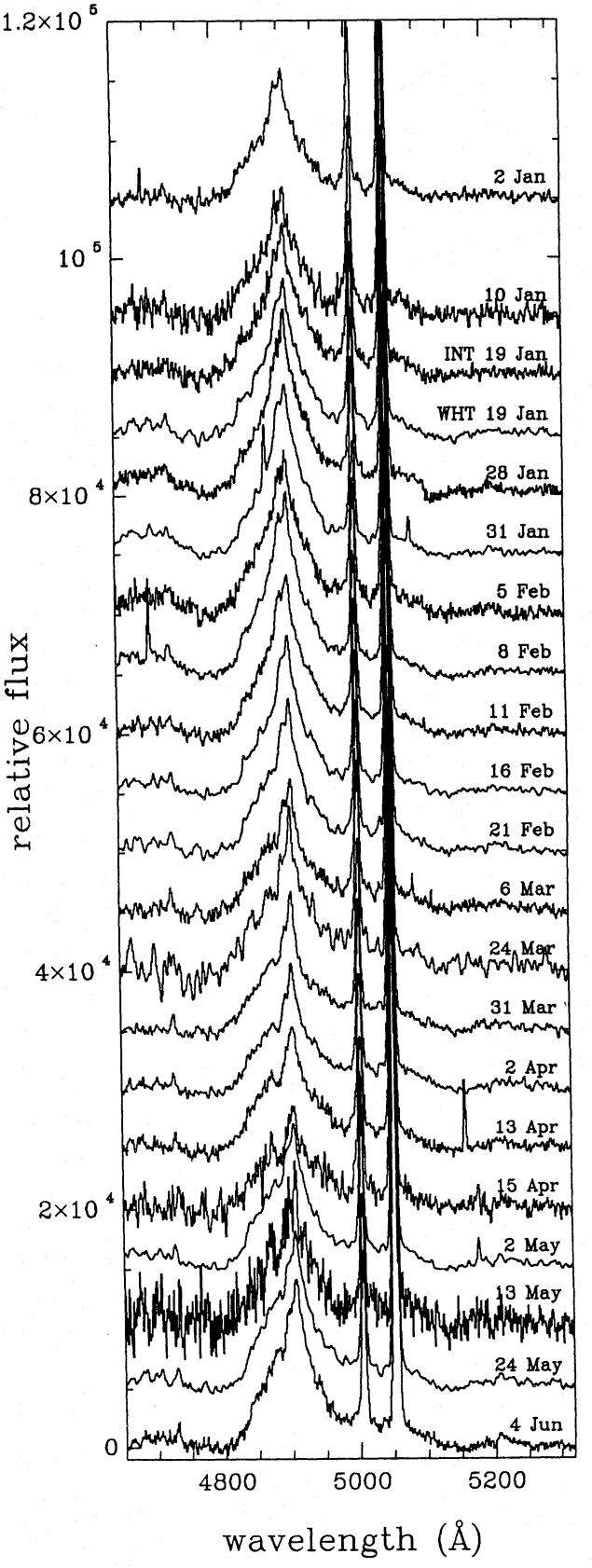

Fig. 4. The Hβ spectra

in the sense that χ^2 increases when the residuals increase. We define the parameter values belonging to the voxel with minimum χ^2 as the best fit. From some initial voxel we find the minimum–χ^2–voxel by using a grid search method (see e.g. Bevington 1969) while calculating the χ^2 for every voxel we pass. We thus avoid calculating a large data cube and the grid can be adjusted easily to allow an accurate solution. This is done in an automatic and thus objective way.

It must be emphasized that by fitting the wavelength region around the narrow lines in the difference spectra with a second order polynomial we are insensitive to any continuum variations or even small slope variations in the background as can be the case when the narrow lines lie in the far wing of varying broad lines. Our scaling method is better than a few percent and can be as good as 1 to 2% in the case of our highest S/N spectra and when the broad lines of the two spectra had approximately the same flux. Several tests show that this method is more accurate than scaling methods based on measuring the narrow-line fluxes (van Groningen & Wanders 1992).

To scale the Hβ spectra we used the (observed) wavelength region 4980 – 5080Å around the [O III] lines and for the Hα spectra the region 6740 – 6820Å around the [S II] lines. We decided to use the [S II] lines instead of the stronger [N II] lines because the [N II] lines fall on the central part of the broad Hα profile and this region is highly variable. The background in the difference spectra around the [N II] lines cannot be fitted by a simple second order polynomial and higher order fitting functions than a first or second order polynomial (to cope with slight curvature in the background) are not desirable.

Figures 3 and 4 present all the scaled Hα and Hβ spectra. Each spectrum has been given an offset for display purposes.

This same scaling procedure was used to subtract the underlying-galaxy template spectrum from the Hβ spectra as discussed in Sect. 3.2. Here, the wavelength region from 5180 – 5330Å was used where several absorption features are visible, including the Mg b lines. The resolution of the galaxy spectrum was not changed since the galaxy-template spectrum had a worse resolution than any individual spectrum.

3.4. The effect of the seeing on the spectra; narrow-line removal

The NLR of NGC 3516 (Pogge 1989; Miyaji et al. 1992) extends over more than 20″ and is clearly resolved in our spectra. The position angle of the slit was kept fixed during the observing campaign and was along the two NLR blobs (position angle 25°, see Pogge (1989) for details in the structure of this NLR). The spatial [O III] profile is shown in Fig. 5. Only the central 2″ are included in the nuclear spectra. A difficulty in scaling spectra to each other in objects like NGC 3516 which possess a resolved NLR, is the effect seeing has. The amount of narrow-line flux entering the aperture will depend on seeing; under bad seeing conditions the amount of narrow-line flux relative to the unresolved continuum and broad-line flux will be larger than under good seeing conditions. We thus have to correct the final fluxes for the differences in seeing during the observations. To find

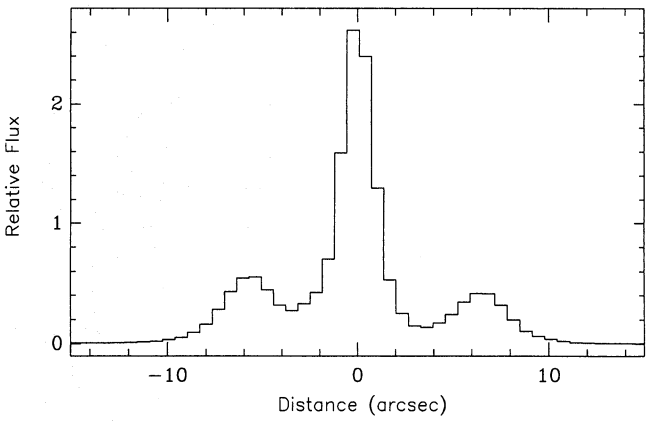

Fig. 5. The spatial [O III] profile

these correction factors we simulated the effect of seeing using a narrow-band [O III] image of NGC 3516 taken with the 3.6m Canada-France-Hawaii Telescope at Mauna Kea on Hawaii with a seeing of 0.″7. The [O III] image was convolved with Gaussian profiles with various widths to simulate observations under different seeing conditions. The total narrow-line flux entering the aperture was then calculated, as well as the total flux from a point source, a star in the same field as NGC 3516, entering the aperture. The ratio of these two is a measure of how much more point-source (broad-line and continuum) flux than narrow-line flux we lose from the aperture when the seeing degrades. The correction factor ϕ^* can then be defined as

$$\phi^*(\boldsymbol{R}, s)\phi_0(\boldsymbol{R}) = \frac{F_{5007}(\boldsymbol{R}, s)}{\Gamma(\boldsymbol{R}, s)}.$$

Here, $\boldsymbol{R}$ is the aperture geometry, s a measure of the seeing, $F_{5007}(\boldsymbol{R}, s)$ the total narrow-line flux entering the aperture and $\Gamma(\boldsymbol{R}, s)$ the total point-source flux entering the aperture. $\phi_0(\boldsymbol{R})$ is a normalizing factor such that $\phi^* = 1$ for the best seeing available; 0.″7 in our case. Using this definition we can just multiply all spectra by the appropriate ϕ^*. This procedure is described in detail in Wanders et al. (1992).

From the 2D spectra we extracted a seeing profile by subtracting the spatial continuum profile from the spatial broad-line profile (a spatial cut through the wings of the broad Hβ and Hα lines, carefully avoiding the spatially extended narrow lines). The result is a spatial point-source profile. It turned out to be very nearly Gaussian; its FWHM was thus identified with the FWHM of the seeing disc.

Table 2 presents the seeing values and the correction factor ϕ^* (taken from Wanders et al. 1992) to be applied to the spectra. We see that the seeing affects the narrow-line strengths by up to 12% for the bulk of the data. The error on the correction factor is about 3%.

After multiplying the spectra with the seeing correction factor, the narrow lines will not vanish in difference spectra. We therefore have to decompose the spectra and subtract the narrow lines. Since, before applying the seeing correction, all spectra were scaled using the assumption that the narrow-line flux is constant over the time interval of interest, we subtracted from

Table 2. Seeing values and correction factors for the spectra

Hβ			Hα		
JD	seeing(″)	ϕ^*	JD	seeing(″)	ϕ^*
7894.59	2.1	1.11	7894.58	2.2	1.11
			7897.61	2.1	1.11
7902.60	3.4	1.20	7902.58	3.0	1.18
7911.63	2.5	1.14	7911.60	2.3	1.12
7911.66	2.3	1.12	7911.68	2.2	1.11
7920.64	1.3	1.04	7920.51	1.6	1.06
7923.60	1.6	1.06	7923.61	1.5	1.06
7928.64	2.2	1.11	7928.62	1.6	1.06
7931.60	1.1	1.01	7931.56	1.4	1.04
7934.50	1.5	1.05	7934.47	1.4	1.04
7939.56	1.3	1.04	7939.54	1.4	1.04
7944.61	1.1	1.01	7944.59	1.9	1.08
7957.51	1.2	1.04	7957.48	2.6	1.15
7975.61	2.0	1.10	7975.48	2.0	1.10
7982.64	1.5	1.05	7982.58	1.5	1.05
7984.49	1.5	1.05	7984.48	1.4	1.04
7995.46	1.5	1.05	7995.44	1.6	1.06
7997.44	4.6	1.31	7997.42	2.6	1.15
8014.40	1.2	1.04	8014.42	1.3	1.04
8025.41	1.5	1.05	8025.44	1.4	1.04
8036.42	1.7	1.07	8032.40	1.5	1.05
8047.41	0.9	1.00	8047.38	0.9	1.00

all spectra the same narrow-line template at fixed wavelengths with fixed strengths. Recall that our χ^2 scaling program shifts and convolves the spectra as well, so that the narrow lines in all spectra, before the seeing correction, have indeed the same strength, the same wavelength and the same resolution.

To find a narrow-line template we made a mean [O III]λ5007 line by averaging the highest S/N Hβ spectra. This line template was then subtracted from all Hβ spectra at 4905.5Å with a relative strength of Hβ/[O III]λ5007 = 0.07, at 5004.3Å with a relative strength of [O III]λ4959/[O III]λ5007 = 0.317 and at 5052.8Å with a strength of unity.

The Hα spectra have been corrected for seeing and narrow lines in the same way as the Hβ spectra, using the same [O III]λ5007-line template. It must be emphasized that the Hα spectra were scaled using the [S II] lines whereas the applied seeing correction factor ϕ^* was deduced from an [O III] image. This procedure is only corrrect if the [S II] and [O III] lines have the same spatial distribution. Because we lack an [S II] image of NGC 3516 we must assume the [S II] spatial distribution is close to that of [O III] and use the [O III]-derived ϕ^* to correct the Hα spectra for seeing effects. We realize a slight error might be introduced here.

3.5. Error propagation

The final error on the flux is calculated as the r.m.s. of the error deduced from our previous data-reduction steps and the error of the seeing correction factor ϕ^*.

Time-series analysis requires knowledge or good estimates of the one-sigma errors on the derived fluxes. Therefore it is important to estimate the flux error for every bin in the raw spectra and let the errors propagate through the data-reduction process, e.g. when shifting, convolving, etc. the spectra. In doing so we assumed the error in one wavelength bin to be independent of the error in neighbouring bins. This, however, is not strictly true, especially in the case of convolving or shifting spectra. The final spectra thus also include a one-sigma flux error for every wavelength bin.

4. Results and discussion

4.1. The light curves

The emission-line light curves The main problem in obtaining line-flux light curves is the measurement of the continuum level in the spectra. No true continuum points can be defined with any certainty. Nevertheless, a rough estimate is made by fitting a power law through three (narrow) wavelength regions in the Hβ spectra where the flux is lowest: 4780 – 4800Å, 5130 – 5150Å and 5300 – 5320Å. The power-law fit is then subtracted from the spectra and all flux in the wavelength region 4824 – 4987Å is added to obtain the total broad Hβ emission-line flux. This wavelength interval corresponds to a velocity interval of −5000 to +5000 km s^{-1} with respect to the peak of the narrow Hβ line. As described in Sect. 3.4 the narrow lines have been subtracted. The errors on the line-flux measurements are mainly the result of the systematic error on the continuum-flux level and

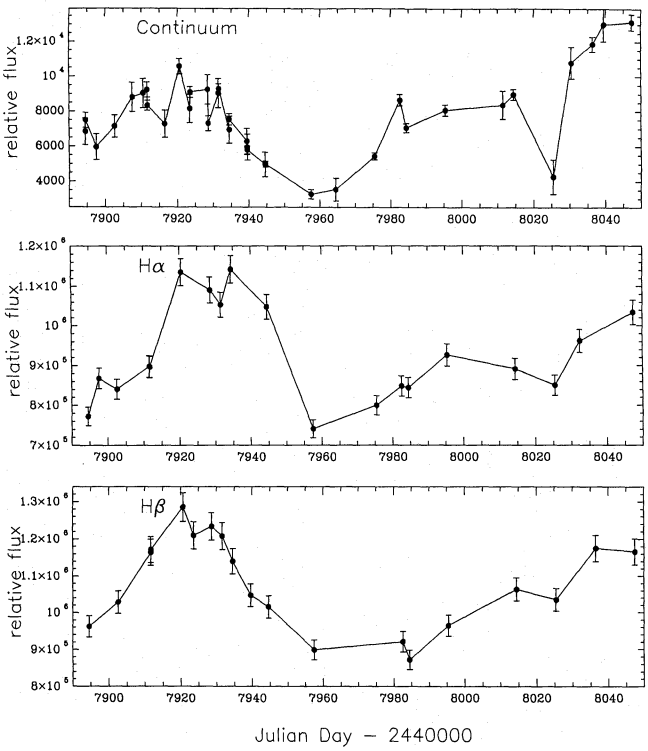

Fig. 6. The continuum and emission-line light curves

the error on the seeing correction factor. For the total Hα line flux all flux was added in the same velocity interval as for the Hβ flux, i.e. -5000 to $+5000$ km s^{-1} with respect to the peak of the narrow Hα line. This corresponds to a wavelength region 6512 – 6732Å. Again, a continuum power-law fit was subtracted and all narrow lines were removed.

The resulting Hα and Hβ emission-line light curves are presented in Fig. 6. These light curves look very similar. Note the almost perfect agreement of the data points of the two nearly simultaneous observations at 19th January (JD 7911.6) of which the difference spectra are given in Fig. 7. One of the observations was done with the INT and the other with the WHT with different instruments. This shows the accuracy of the data reduction. (The narrow-line residuals that are visible were reintroduced after the relative scaling of the spectra by applying the seeing correction and by the narrow-line removal procedure. They do not indicate bad scaling.)

Several points in the light curves deserve some extra attention (ref. Table 3). While observing in the red on the 16 February (JD 7939.5) the observer noted that the "object drifted". Therefore, the aperture will not have been centred on the object and this means we have too little broad-line flux in comparison with the narrow-line flux in our aperture. This is due to the extended nature of the narrow lines (Wanders et al. 1992). This explains the low broad Hα flux measured on 16 February and possibly also on 31 January (JD 7923.6). On 15 April (JD 7997.4) the seeing was extremely bad and unstable. These observations are not reliable in the flux calibration and should not be considered for further analysis. The Hβ observation of 24 March (JD 7975.5) is strange in the sense that it shows an excess broad-

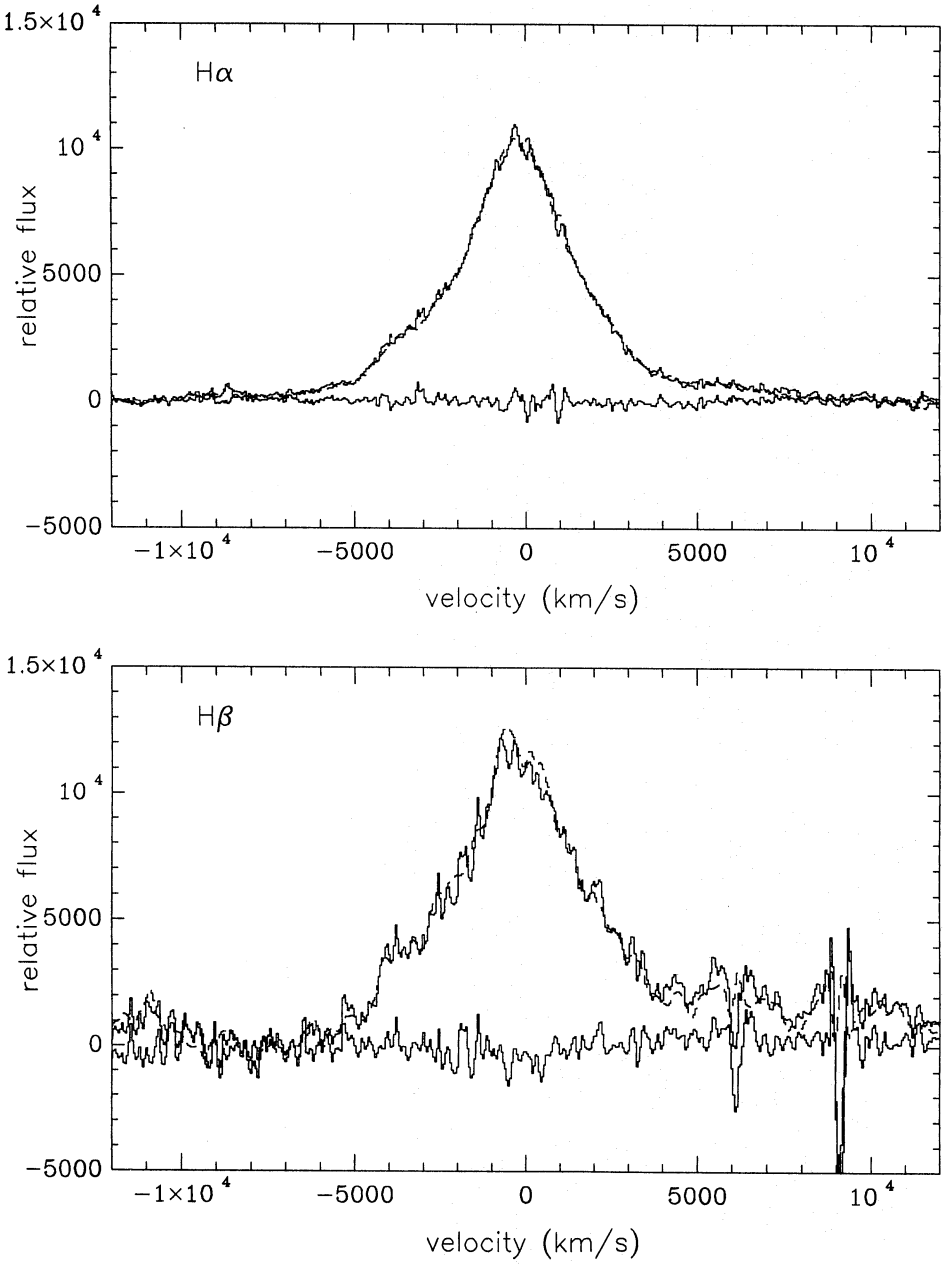

Fig. 7. Difference spectra of Hα and Hβ of the nearly simultaneous observations at 19 January. The two observations give to within the error in the continuum flux level exactly the same result. The INT spectra are shown in a solid line, the WHT spectra in a dashed line

Table 3. The continuum, Hβ and Hα light-curve data

JKT Photometry			blue spectrometry						red spectrometry					
	Continuum			Continuum		Hβ				Continuum		Hα		
JD	Flux	σ	JD	Flux	σ	Flux	σ	W_λ (Å)	JD	Flux	σ	Flux	σ	W_λ (Å)
7894.50	68.4	2.1	7894.59	74.8	4.3	96.2	3.0	129 ± 8	7894.58	72.0	3.4	77.2	2.3	>173 ± 8
7897.50	59.6	1.8							7897.61	79.0	3.6	86.8	2.6	>181 ± 8
7907.50	88.2	2.6	7902.60	71.4	6.3	102.9	3.3	144 ± 14	7902.58	85.7	3.9	84.1	2.5	>165 ± 8
7910.50	90.4	2.7	7911.63	92.3	4.3	116.5	3.5	126 ± 7	7911.60	88.4	4.3	89.8	2.7	>172 ± 8
7916.50	72.8	2.2	7911.66	83.4	2.9	117.2	3.5	141 ± 6	7911.68	76.6	3.2	89.7	2.7	>192 ± 8
			7920.64	105.8	4.4	128.6	3.9	122 ± 6	7920.51	86.6	3.7	113.5	3.4	>221 ± 10
7923.50	81.6	2.4	7923.60	91.0	3.1	121.0	3.6	133 ± 6	7923.60			95.2	2.9	>221 ± 10
7928.50	92.6	2.8	7928.64	73.2	4.3	123.4	3.8	169 ± 11	7928.62	79.1	3.6	109.1	3.3	>228 ± 10
7931.50	90.4	2.7	7931.60	92.8	3.0	120.8	3.6	130 ± 6	7931.56	72.7	3.3	105.3	3.2	>234 ± 11
7934.50	69.5	2.1	7934.50	75.4	3.2	114.0	3.4	151 ± 8	7934.47	80.3	3.6	114.2	3.4	>236 ± 11
7939.45	62.9	1.9	7939.56	58.0	2.3	104.7	3.2	181 ± 9	7939.54			81.1	2.4	>222 ± 10
7939.55	59.6	1.8												
7944.50	49.7	1.5	7944.61	49.9	1.7	101.6	3.1	203 ± 9	7944.61	72.1	3.0	104.8	3.1	>234 ± 10
			7957.51	32.6	2.7	89.9	2.7	276 ± 25	7957.48	58.0	2.5	74.1	2.2	>194 ± 8
			7975.48	54.4	1.9	116.8	3.5	215 ± 10	7975.48	65.8	2.8	80.0	2.4	>191 ± 8
			7982.64	86.5	3.3	92.1	2.8	107 ± 5	7982.58	61.3	3.1	84.9	2.6	>213 ± 10
			7984.49	70.6	2.6	87.2	2.6	124 ± 6	7984.48	52.0	2.8	84.4	2.5	>238 ± 11
			7995.46	80.6	3.2	96.5	2.9	120 ± 6	7995.44	74.3	3.2	92.6	2.8	>203 ± 9
			7997.42	35.2	3.0	94.7	2.9	269 ± 24	7997.44			76.0	2.3	>174 ± 8
8011.50	83.8	2.5	8014.40	89.8	3.1	106.4	3.2	119 ± 5	8014.42	62.7	3.3	89.2	2.7	>221 ± 11
			8025.41	42.7	9.9	103.5	3.6	243 ± 57	8025.44	55.8	7.0	85.0	2.7	>228 ± 21
8030.50	108.0	3.2	8036.42	118.7	4.2	117.5	3.6	99 ± 5	8032.40	78.8	3.6	96.2	2.8	>201 ± 9
8039.50	130.0	3.9	8047.41	131.4	4.6	116.6	3.5	89 ± 4	8047.38	83.5	3.6	103.4	3.1	>207 ± 9

Hβ flux which we cannot explain. Seeing and miscentring the aperture will reduce the ratio of broad-line to narrow-line flux and not vice versa. For any further analysis for which the flux calibration is important we ignore all observations of 15 April, the Hβ observation of 24 March and the Hα observations of 31 January and 16 February.

The continuum light curves We have three independent light curves that represent three different parts of the continuum spectrum of NGC 3516: The JKT B-band light curve (LCV_{JKT}) and the light curves of the continua around Hβ and Hα as derived from the spectra (LCV_{blue} and LCV_{red} respectively).

LCV_{JKT} also includes the emission lines Hδ and Hγ. He IIλ4686 is weak in NGC 3516 and falls at the edge of the Johnson-B filter where the transmission is low. From an old spectrum of NGC 3516 (Pérez, private communication) we find that the relative equivalent widths of Hδ/Hβ and Hγ/Hβ are ~ 0.13 and ~ 0.25 respectively. In a bright state the equivalent width of Hβ is found to be $\sim$ 200Å and thus the equivalent widths of Hδ and Hγ are $\sim$ 34Å and $\sim$ 64Å respectively. Thus, together these lines contribute to $\sim 1/11$ of the total flux measured through the Johnson-B filter (which has an effective width of $\sim$ 900Å) and the error on the continuum-flux measurement, due to emission lines, must be less than $\sim 9\%$. If we then take into account that $\sim 70\%$ of the Hβ and Hα emission-line flux is constant over the time spanned by our monitoring campaign and this, most likely, also will be the case for Hγ and Hδ, we reduce the error on the variability of the continuum that is due to variable emission lines, to less than $\sim 2.7\%$. The stellar contribution to the LCV_{JKT} can be assumed constant as the FWHM of the seeing disc was always well below the aperture size.

Both the LCV_{blue} and LCV_{red} have been defined as the corresponding flux of the power-law fit at the wavelengths of the narrow Hβ and Hα lines, i.e. at 4905Å and 6622Å respectively. Recall that the stellar contribution to LCV_{blue} has been subtracted whereas the stellar contribution to LCV_{red} is $\sim 40\%$, as deduced from an old spectrum of NGC 3516, and variable with seeing.

Intercalibration of the continuum light curves The spectral and photometric continuum-source light curves are assumed to form homogeneous data sets. We can thus scale them to each other using a least-squares fit of the simultaneously observed data points in the light curves. The blue and JKT light curves are very similar which strengthens our conclusion that the method of subtracting the underlying galaxy spectrum can be done accurately. Since the blue-continuum light curve does not contain any galactic star light, fitting the JKT light curve to the same scale means we automatically get rid of the constant contribution of the underlying galaxy in the photometry data.

The red-continuum light curve can also be scaled to the blue one in the same way as the JKT light curve. Again, we get rid of the constant part of the underlying galaxy. However, the red curve also contains a variable part from the underlying galaxy, due to seeing effects, which can not be scaled away. A consistency check can be made, though. After scaling the red curve to the blue one we can check the residuals of the blue and red curves and see if they correlate with seeing as would be expected. The blue curve comes from a point source only whereas the red curve comes from a point source plus an extended source (the galaxy). Under worse seeing conditions we therefore expect there to be more red flux relative to blue flux than under better seeing conditions. Doing this test shows that the residuals indeed correlate with seeing in the expected manner. Because of the seeing-dependent underlying-galaxy component we will not use the red continuum light curve in further analysis but merely note its consistency with the blue and JKT-continuum light curves.

All resulting light-curve data are summarized in Table 3; the flux is in arbitrary units. The quoted σ is the one-sigma error on the flux, deduced from the S/N of the spectra, the error on the scaling procedures, the error on the seeing correction factor, and the error on the determination of the continuum level. The equivalent width W_λ is given in Ångström. For Hα, only a lower limit on the equivalent width can be given because the continuum is contaminated by a stellar contribution. The combined JKT and blue continuum light curves and the emission-line light curves are plotted in Fig. 6.

Note that the Hα data were reduced completely independently from the JKT and blue-continuum data, as well as the Hβ line-flux data, and therefore no correlated reduction errors between these can exist.

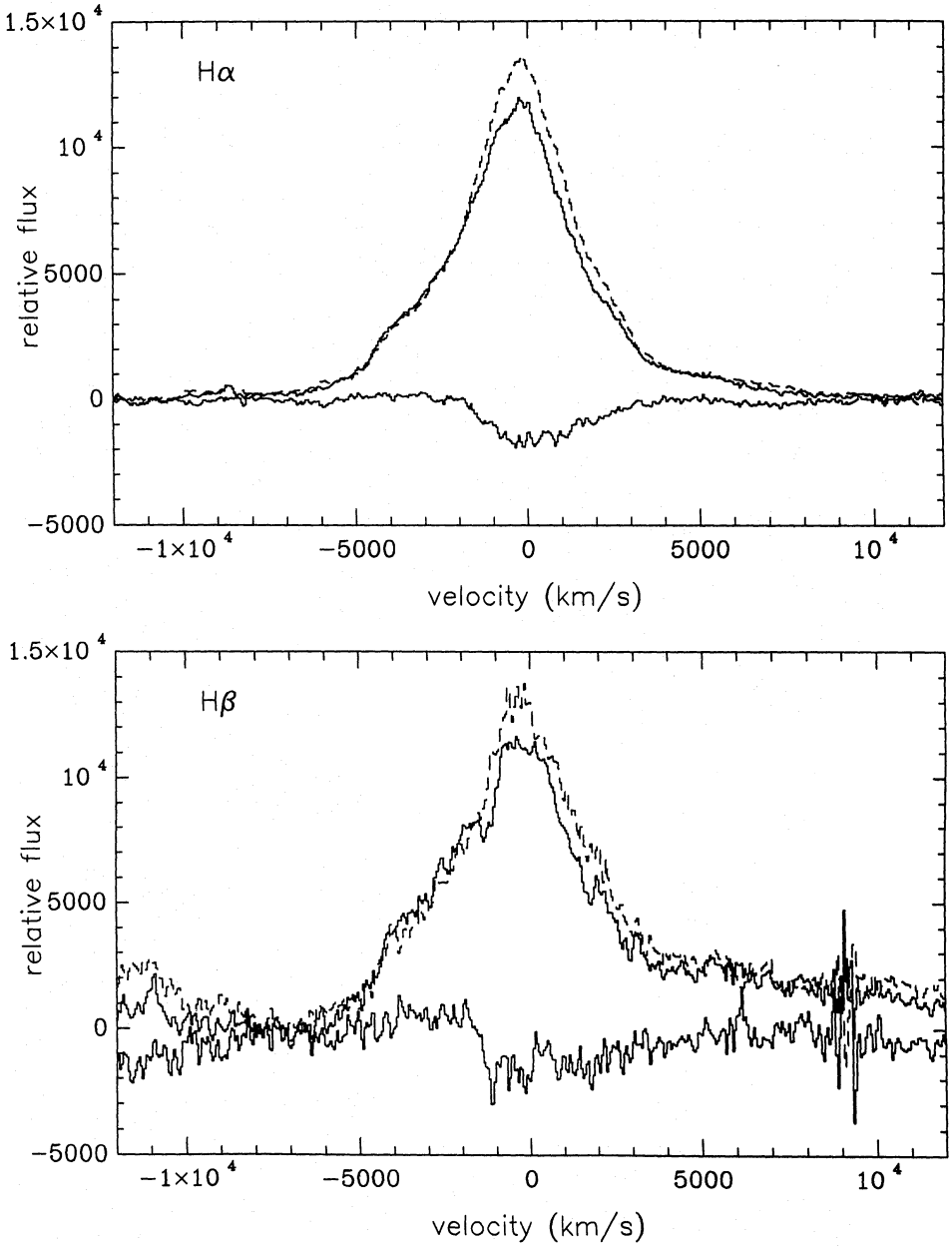

Fig. 8. Difference spectra of Hα and Hβ of 4 June (solid line) and 28 January (dashed line)

4.2. Difference spectra

Subtracting two spectra from each other is one of the best ways of evidencing broad-line variations. Since all narrow emission lines are subtracted from the nuclear spectra these do not show up in the difference spectra and we are left with only broad-line variations. From our difference spectra we find that any significant asymmetric profile variations do not occur on short time scales. However, on time scales of several weeks large variations occur. Two examples are given in Figs. 8 and 9 where the difference spectra are shown for 4 June and 28 January and 4 June and 31 March respectively. Not only these examples, but all difference spectra show that the Hα and Hβ profile variations resemble each other closely.

4.3. Spectral features

A prominent feature, best described as a dip, emerges on the blue wing of Hβ during the campaign. It is first visible in the 21 February spectrum and best visible in the 13 April spectrum. It can be seen that it does not vary in ("absorbed") flux simultaneously with the continuum or line flux. The dip is about 1290 km s^{-1} blueward of the narrow Hβ emission-line peak and is at the same blueward velocity shift as the absorption features in the UV lines in this object (Ulrich 1988; Voit et al. 1987; Walter et al. 1990). All our spectra showing this absorption feature (i.e from 21 February to 4 June) were added and this mean spectrum is shown in Fig. 10 together with a C IV emission-line profile as observed by IUE in 1982, i.e. eight years earlier than the Hβ observation. Clearly in both lines this dip is visible at the same velocity shift.

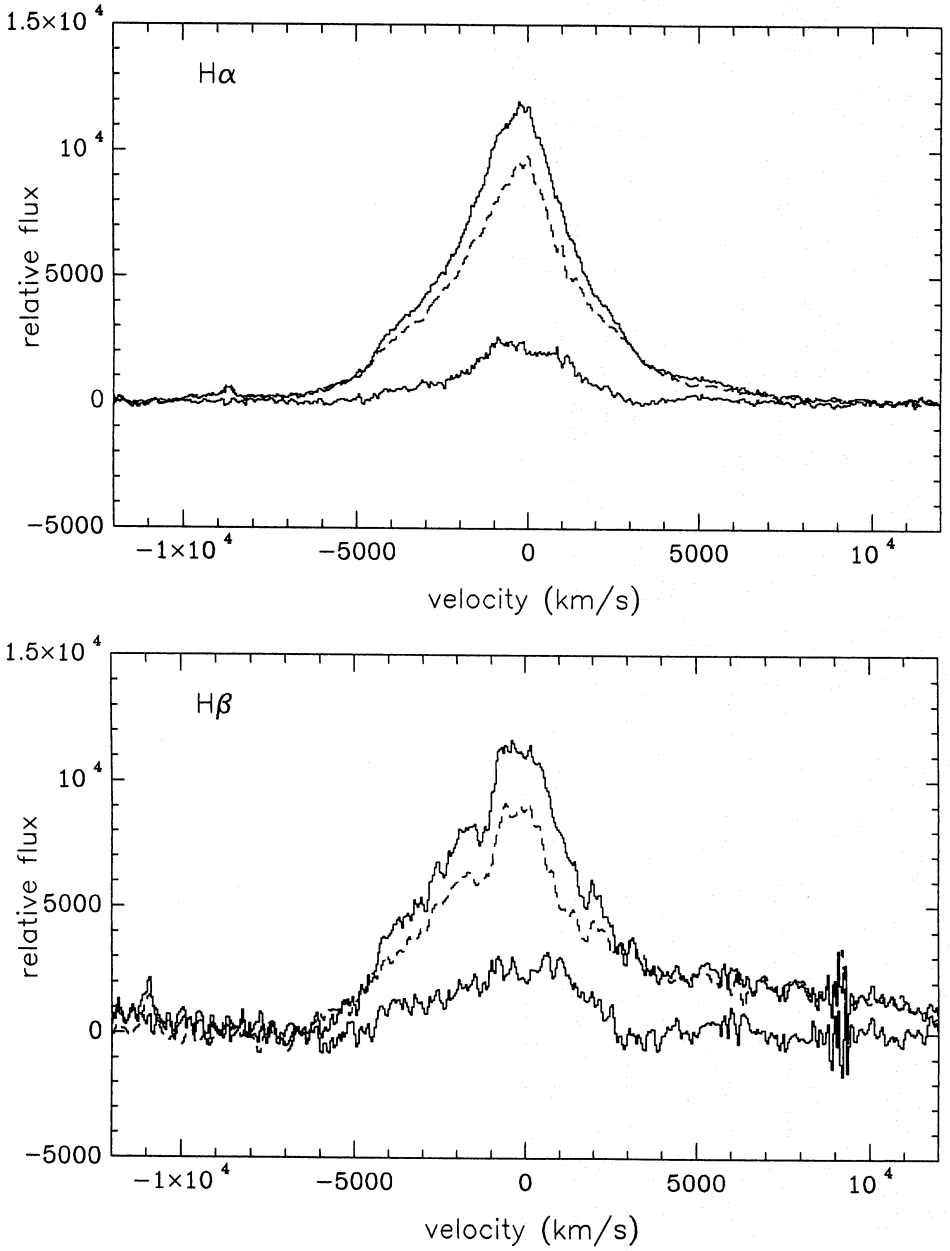

Fig. 9. Difference spectra of Hα and Hβ of 4 June (solid line) and 31 March (dashed line)

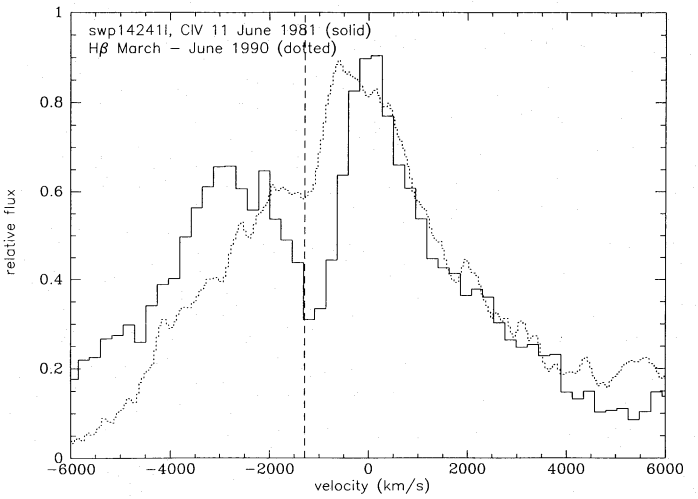

Fig. 10. The mean Hβ profile with dip and a C IV profile as observed by IUE in 1981

If a dip in the Hα profile were present at the same velocity as the one in the Hβ and UV spectra it would be more difficult to observe since the narrow [N II]λ6548 emission line falls at the same wavelength. In Hβ, the dip is present in all spectra after 21 February. We therefore made two mean Hβ spectra, one with all spectra from before 21 February and one with all from after 21 February. We did the same for Hα. To test whether the dip is also present in the Hα line, we made difference spectra of these mean spectra. Since the Hα variations generally resemble the Hβ variations, the hypothesis is that if this Hα difference spectrum closely resembles its Hβ equivalent, the dip is present in both lines. These two difference spectra are shown in Fig. 11 and it is immediately clear that these look similar except for the absorption-like feature on the wing of Hβ. We therefore conclude that the dip is not detected in Hα. Also the narrow-line subtracted Hα profiles, as presented in Fig. 11, show no sign of a dip similar to the one in Hβ. This imposes stringent limits on any theory explaining this dip as absorption. If it were not

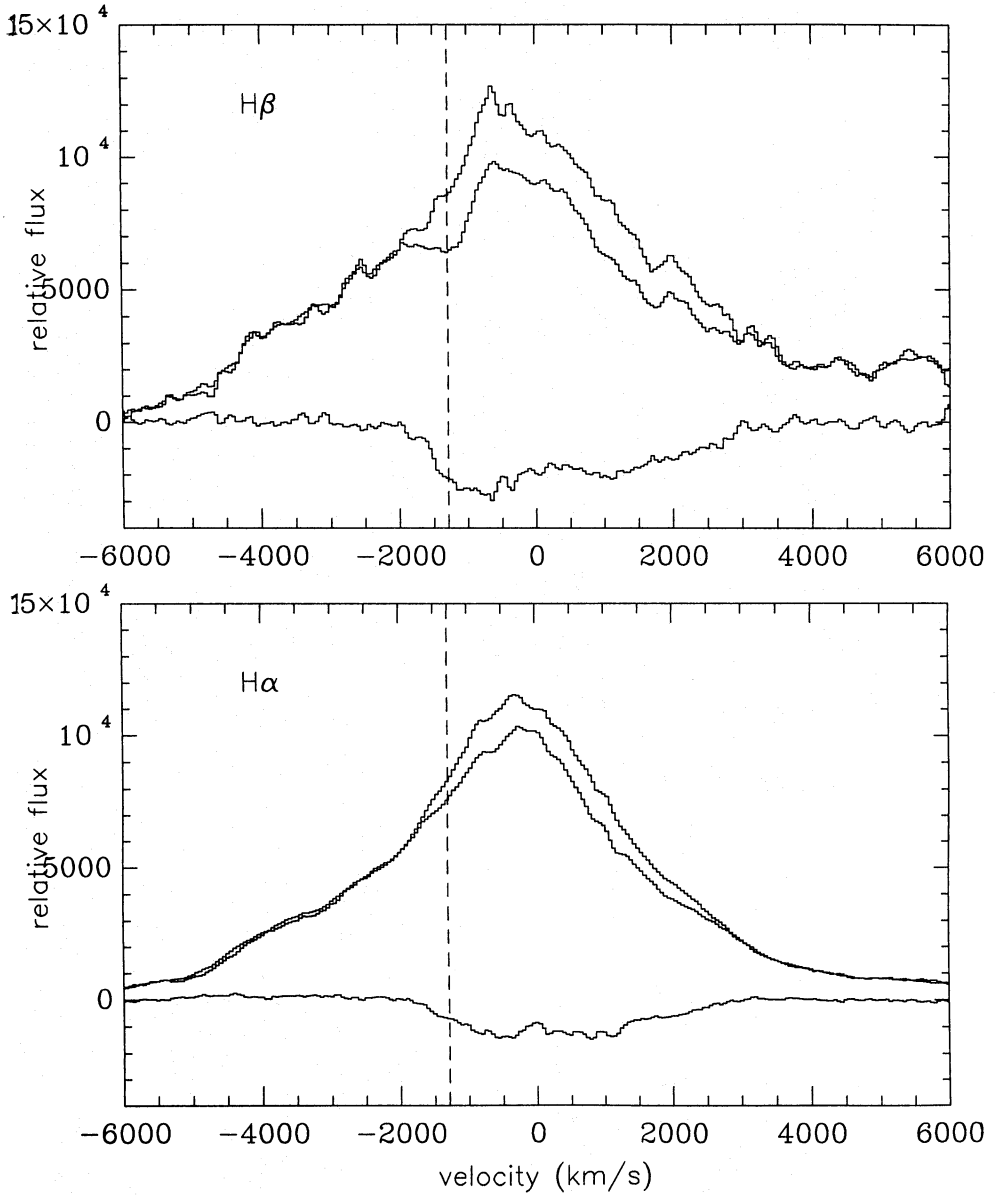

Fig. 11. The Hα and Hβ difference spectra of all spectra with (all spectra after 21 Feb.) and without (all spectra before 21 Feb.) dip in the Hβ profile

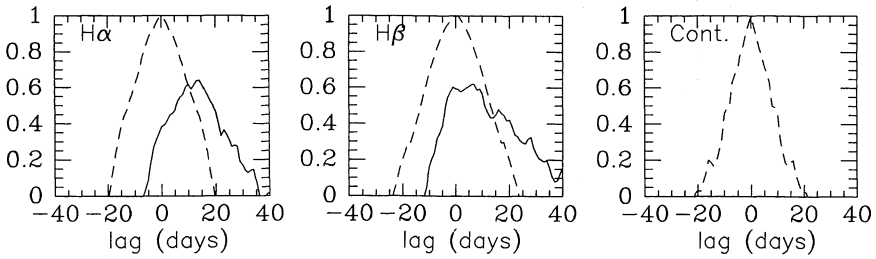

Fig. 12. The auto-correlation functions of the continuum and emission-line light curves (dashed lines) together with the cross-correlation functions (solid lines) of the Hα and Hβ light curves versus the continuum light curve

absorption but a trough between two emission peaks, the fact that it is not seen in the Hα profile implies that the ionizing conditions in the part of the BLR responsible for the material at the position of the dip are radically different from elsewhere in the BLR.

The peaks of both the broad Hα and Hβ line are blue shifted with respect to the peak of the narrow line; the broad Hα line by $\sim 200 \pm 100$ km s^{-1} and the broad Hβ line by $\sim 400 \pm 100$ km s^{-1}.

The small absorption feature at $\sim$ 6550Å in the far blue wing of Hα is probably a blend of CaIλ6493.8 and FeIλ6495.0 in the underlying galaxy spectrum and has nothing to do with the BLR.

4.4. Cross-correlation analysis

An estimate of the size of the BLR is generally inferred from the cross-correlation function (CCF) of the emission-line light curve with the continuum light curve. The position of the peak in the CCF is associated with the inner boundary of the BLR, and the position of its centroid with the luminosity-weighted radius of the BLR (Koratkar & Gaskell 1991). An upper limit to the size of the BLR can be obtained from the width of the auto-correlation function (ACF) of the emission-line light curves.

We used the cross-correlation method developed by Gaskell & Sparke (1986) and Gaskell & Peterson (1987) and found for NGC 3516 that the overall size of the BLR, as inferred from the ACF, is less than $\sim$ 26 light days for Hα and less than $\sim$ 28 light days for Hβ. From the line versus continuum CCFs we estimate the inner radius of the BLR to be 14 ± 3 light days for Hα and 7 ± 3 light days for Hβ. The centroids of the CCFs yield luminosity-weighted radii of 14 light days for Hα and 11 light days for Hβ. Note that the true radii may be slightly under-estimated by this analysis, as shown by Pérez et al. (1992). The CCFs and ACFs are presented in Fig. 12 together with the ACF of the continuum source. Because the line ACFs are much wider than the continuum ACF, the line ACFs and CCFs are not dominated by undersampling effects. Our inferred size of the BLR in NGC 3516 is a factor two smaller than the size found by Cherepashchuck & Lyutyi (1973).

5. Summary

We have shown that the Seyfert-1 galaxy NGC 3516 shows large flux variations on a time scale of several weeks. Asymmetric profile variations occur on the same time scale. We have shown the presence of a varying dip in the Hβ emission-line profile which is similar to the absorption features seen in the UV emission lines of NGC 3516. The dip is not present in the Hα emission line which imposes strong limits on the physical nature of the material responsible for this feature. We derived a size of the BLR of 14 ± 2 days.

Acknowledgements. We are indebted to Drs. B.M. Peterson, R.W. Pogge and M.M. DeRobertis for providing us the excellent narrow-band [O III] image which was essential for this study. The CCI is thanked for the allocation of international observing time awarded to the LAG. We acknowledge the help, support and patience of the staff at the La Palma Observatory. The numerous observers who took part in this LAG monitoring program thank the national funding agencies who generously supported them, including the NFR, SERC, ESA, RGO, DFG and CNRS. The IAC is thanked for providing support and assistance for distribution and initial reduction of the data. Their hospitality is gratefully acknowledged. The JKT, INT and WHT are operated on the island of La Palma by the Royal Greenwich Observatory at the Spanish Observatorio del Roque de los Muchachos of the Instituto de Astrofísica de Canarias.

Appendix A: NGC 3516 Fughetta

Once upon a time during a conference an idea arose of transforming light curves into sound curves. Active Galactic Nuclei are particularly attractive because the line light curves follow the continuum light curve with a delay, introducing an echo. We decided to try the experiment with the derived light curves of NGC 3516 before seeing correction, i.e. as they are observed.

We filled in the gaps of the light curves by using a maximum entropy method in order to obtain light curves which are defined for every day. We rebinned the intensity scale of the three light curves (continuum, Hβ and Hα) into a linear scale of 24 bins. We identified each of these bins with a musical note, the minimum with the low C and so upward. This fills exactly two octaves on an atonic scale. Each day in the light curves was identified with a quaver. We defined 160 days in each of the light curves so this made 40 bars.

We let the driving continuum light curve be played by a cello, the Hβ light curve by a violin and the Hα light curve by a piano. It should be played four times: the first time only by the cello, the second time by the cello and violin and the third and fourth time by the cello, violin and piano.

Special thanks to Nils Bergvall who helped editing and operating the synthesiser.

NGC 3516 Fughetta

December 1991

Adagio ♩ = 50

Violin

Cello

Piano

1, 2, 3

4

References

Andrillat Y. and Souffrin S., 1968, Astrophys. Lett. 1, 111

Baribaud T. and Alloin D., 1990, A&A 236, 346

Bevington, 1969, Data Reduction and Error Analysis for the Physical Sciences, New York, McGraw-Hill

Bica E., 1988, A&A 195, 76

Blandford R.D. and McKee C.F., 1982, ApJ 255, 419

Cherepashchuck A.M. and Lyutyi V.M., 1973, Astrophys. Lett. 13, 165

Clavel J. et al., 1991, ApJ 366, 64

Gaskell C.M. and Sparke L.S., 1986, ApJ 305, 175

Gaskell C.M. and Peterson B.M., 1987, ApJS 65, 1

Jackson et al., 1992, A&A, in press

Koratkar A.P. and Gaskell C.M., 1991, ApJS 75, 719

Maoz D., Netzer H., Mazeh T., Beck S., Almoznino E., Leibowitz E., Brosch N., Mendelson H. and Laor A., 1991, ApJ 367, 493

Miyaji T., Wilson A.S. and Pérez-Fournon I., 1992, ApJ 385, 137

Oke J.B. and Gunn J.E., 1983, ApJ 266, 713

Pérez E., Robinson A. and de la Fuente L., 1991, in: Variability of Active Galaxies, eds. Duschl W.J., Wagner S.J., Camenzind M., p.97

Pérez E., Robinson A. and de la Fuente L., 1992, MNRAS 255, 502

Peterson B.M. et al., 1991, ApJ 368, 119

Peterson B.M., Ali B., Horne K., Bertram R., Lame N., Pogge, R.W. and Wagner, R.M., 1993, ApJ 402, in press

Pogge R.W., 1989, AJ 98, 124

Stirpe G.M., de Bruyn A.G. and van Groningen E., 1988, A&A 200, 9

Ulrich M.-H., 1988, MNRAS 230, 121

van Groningen E. and Wanders I., 1992, PASP 104, 700

Voit G.M., Shull, J.M. and Begelman, M.C., 1987, ApJ 316, 573

Walter R., Ulrich M.-H., Courvoisier T.J.-L. and Buson L.M., 1990, A&A 233, 53

Wanders I., Peterson B.M., Pogge R.W., DeRobertis M.M. and van Groningen E., 1992, A&A, in press

Welsh W.F. and Horne K., 1991, ApJ 379, 586

This article was processed by the author using Springer-Verlag TEX A&A macro package 1992.